Received: 3 April 2022 | Accepted: 19 May 2022

DOI: 10.1002/bab.2374

WILEY

ORIGINAL ARTICLE

Evaluating glioma-associated microRNA by complementation on a biological nanosensor

Zizhuo Li | **Xin Wan** | **Mingming Li** | **Qiuxia He** | **Haichao Yang** | **Wei Zhang** | **Xiuhua Yang**

Department of Abdominal Ultrasound, The First Affiliated Hospital of Harbin Medical University, Harbin city, Heilongjiang Province 1, China

Correspondence
Xiuhua Yang, Department of Abdominal Ultrasound, The First Affiliated Hospital of Harbin Medical University, Harbin city, Heilongjiang Province, 150001, China.
Email: yangxiuhua0818@sina.com

Zizhuo Li and Xin Wan equally contributed to this study.

Abstract

Glioma is a tumor in the brain and spinal cord originating in the glial cells that surround the nerve cells. Among several microRNAs reported, miRNA-363 is associated with human glioma. Based on miRNA-363 levels, the development and progression of glioma can be monitored. The current study used an interdigitated electrode sensor to monitor microRNA-363 levels, which indeed reflects the severity of glioma. The interdigitated electrode was generated using a photolithography technique followed by surface chemical modification carried out to insert miRNA-363 complementary oligo as the probe complexed with gold nanoparticles. The proposed sensor works based on the dipole moment between two electrodes, and when molecular immobilization or interaction occurs, the response by the signal output changes. The changes in the target microRNA-363 sequence were standardized to identify glioma. The limit of detection of miRNA-363 was 10 fM with an R^2 value of 0.996 on the linear coefficient regression ranges between 1 fM and 100 pM. Furthermore, unrelated sequences failed to increase the response of the current with the complementary probe, indicating specific miRNA-363 detection on the interdigitated electrode. This study demonstrates the platform to be used for determining the presence of microRNA-363 in glioma and as the basis for other biomarker analyses.

KEYWORDS
biomarker, biosensor, dielectrode, glioma tumor, miRNA-363

1 | INTRODUCTION

Glioma is a type of common tumor that originates in the brain [1] and is derived from the glial cells (gluey supportive cells) that surround the nerve cells to support neurons, such as oligodendrocytes, astrocytes, and ependymal cells in the brain. Glioma is also called an intra-axial tumor because it can grow within the substance of the brain and spread in normal brain tissue. Glioma can affect brain function and is life-threatening depending on its growth rate. In general, surgery, chemotherapy, radiation therapy, and targeted therapy are the treatments for glioma. Magnetic resonance imaging is an imaging method used to diagnose glioma. However, imaging methods are complicated, expensive, and difficult to access. Therefore,

Abbreviations: miRNA, MicroRNA; fM, femtomolar; pM, picomolar; MRI, Magnetic resonance imaging; BBB, Blood-brain barrier; HDAC-9, Histone deacetylase 9; GAP-43, Growth associated protein 43; RAP-1, Ras-related protein 1; MMP-9, Matrix metalloproteinase-9; APTES, (3-aminopropyl)triethoxysilane); PBS, Phosphate-buffered saline; PEG, Polyethylene glycol; aM, Attomolar; nM, Nanomolar; IDE, Interdigitated Electrode; DNA, Deoxyribonucleic acid.

developing an easy identification method/strategy is needed for glioma diagnosis. Blood-based biomarkers have been effectively used to identify various targets in diagnosing different diseases.[2–5] The diagnosis, treatment, and prognosis of glioma are partly hindered by the presence of the blood–brain barrier (BBB). Simultaneously, a significant number of exosomes are released by glioma, which can escape the BBB and become a systemic biomarker for the progression of glioma.[6,7] Exosomes are extracellular vesicles characterized by the presence of membrane CD9 and CD81 proteins and functional miRNAs. Exosomes play a major role in the intercellular communications between the tumor and normal cells.[8] Identifying biological markers helps in diagnosing glioma and its growth condition. This study focused on detecting miRNA-363, a suitable biomarker for glioma.[9]

MicroRNAs (miRNAs) are phylogenetically preserved small noncoding RNAs that typically contain 21–24 bases and play a vital role in the posttranscriptional regulation of gene expression.[10–12] To date, more than 1000 miRNA targets have been identified, and several of them are promising biomarkers for identifying and classifying various diseases.[13,14] The roles of miRNAs have been demonstrated in many cancer types, including glioma.[15,16] Various miRNAs are greatly involved in the progression of gliomas; for example, overexpression of miRNA-21 in glioma is highly associated with tumor growth through the inhibition of apoptosis.[17] In addition, deregulation of many miRNAs in gliomas is associated with alterations in differentiation, proliferation, and invasion.[18,19] Among other miRNAs, miRNA-363 was uniform and highly overexpressed in glioma. Predicted targets for miRNA-363 are histone deacetylase 9 (HDAC-9), growth-associated protein 43 (GAP-43), and Ras-related protein 1 (RAP-1). miRNA-363 was upregulated in all tumor cell lines and specimens, and the expression of miRNA was highly associated with tumor grade. The transfection of glioma cells with the specific inhibitor of miRNA-363 increased the expression level of the tumor suppressor GAP-43. Furthermore, transfection of glioma cells with the specific anti-miRNA-363 antibody increased GAP-43 expression, suggesting that miRNA-363 is a potential target for glioma.[20] In addition, the inhibition of miRNA-363-induced downregulation of matrix metalloproteinase-9 (MMP-9), MMP-2, AKT, and Bcl-2 plays a major role in the signature of malignant glioma. Therefore, quantifying miRNA-363 helps to diagnose glioma and its causes. This research focused on quantifying miRNA-363 by its target and a complementary sequence on gold nanomaterial-modified interdigitated electrodes.

Nanomaterials applications in the medical field are becoming popular; in particular, nanomaterials in biosensors help to enhance target identification and lower the limit of detection.[21–29] Nanomaterials enhance the surface functionalization of biomolecules on the sensing electrode and improve the stability of biomolecules, helping to increase the interaction of the target and analyte on the sensor surface. Gold is a popular material and is effectively applied in various biosensing applications.[30–35] In most cases, it is used to prepare the sensing electrode and as the linker to attach the biomolecules on the electrode.[36,37] Here, thiolated complementary miRNA-36s were attached to the electrode through Au nanoparticles, and this electrode was used to detect the target miRNA-363. Upon immobilizing Au nanoparticles on the sensing surface, surface physical modification will occur. Ultimately, this will enhance the surface area to accommodate more molecules. For this reason, the current study used Au nanoparticles to immobilize a higher number of probes, which enhanced the number of target interactions.

Highlights

The interdigitated electrode was generated using a photolithography technique followed by surface chemical modification carried out to insert miRNA-363 complementary oligo as the probe. The limit of detection of miRNA-363 was found to be 10 fM with an R^2 value of 0.9912 on the linear coefficient regression ranges between 1 fM and 100 pM.

2 | MATERIALS AND METHODS

2.1 | Biomolecules and reagents

Au nanoparticles (15 nm), ethanol, APTES ((3-aminopropyl)triethoxysilane), phosphate-buffered saline (PBS; pH 7.4), and human serum were obtained from Sigma Aldrich (USA). The following sequences were used as the target and complement of miRNA-363 and were commercially synthesized by the local supplier.[9] Target: 5′-linker-GGTTTACAGATGGATACCGUGCAATTTTTCTCCUATGATACTCATCAAAATTGCATCGTGATCCACCCGACAACA-3′; complementary: 5′-UGUUGUCGGGUGGAUCACGAUGCAAUUUUGAUGAGUAUCAUAGGAGAAAAAUUGCACGGUAUCCAUCUGUAAACC-3’; random sequence: 5′-GAGGUGAAAAGUUCGAUAAAAAAGGCCCCAGCAGUCGGAAAAAGCUCCCGGCCUUCCAACGCAAACCAGCGGGAA-3′.

2.2 | Interdigitated electrode preparation

The traditional wet-etching method was used to prepare the interdigitated electrode surface.[38,39] A silicon wafer was used as the base, and aluminum was deposited on the silicon wafer. First, the standard cleaning procedure was performed on the base silicon wafer, and then the oxidation process was conducted to cover the surface with silicon dioxide. On the oxidized surface, aluminum was coated by a thermal evaporator, and the photoresist was further deposited by the spin coating method (1200 rpm for 10 s, 3500 rpm for 20 s, and 500 rpm for 10 s). Then, the pattern was transferred to the aluminum surface by ultraviolet exposure. The unexposed regions were eliminated by photoresisting and then heating the electrode to 100°C to remove the excess moisture and strengthen the adhesion between aluminum and SiO_2. Then, the electrode was etched with an aluminum etchant to remove the unexposed area. Finally, the fabricated Interdigitated electrode (IDE) was cleaned with acetone and distilled water.

2.3 | Conjugation of Au nanoparticles with complementary sequences

The thiol-terminated complementary sequence was conjugated with Au nanoparticles and then fixed on the electrode using an amine linker. For this conjugation process, 50 μL of as-received Au nanoparticles was mixed with a 2-μM probe and kept for 1 h, and then the conjugated Au nanoparticles were separated by centrifugation at 10,000 *g* for 10 min. The separated Au nanoparticle-conjugated complementary probe (Au nanoparticle-probe) conjugate was washed with distilled water and stored in a refrigerator (4°C) for the surface functionalization process.

2.4 | Functionalizing electrode by a complementary probe through Au nanoparticle

An Au nanoparticle probe was attached to the electrode with an amine linker. The following steps were conducted for the immobilization process: (i) The electrode was immersed in KOH at 1% for 10 min; (ii) diluted 1% APTES was added to the IDE, rested for 3 h, and immersed in 30% ethanol to remove the excess APTES; (iii) 5 μL of Au nanoparticle-probe was placed and left for 1 h. (iv) PEG-COOH was used to block the excess APTES; (v) target miRNA-363 sequence was added. In between each process, the electrode was washed with PBS, and then the current response was recorded.

2.5 | Quantification of miRNA-363 target duplex formation

miRNA-363 target was quantified on the Au nanoparticle-probe attached electrode. For this experiment, miRNA-363 concentrations from 100 aM to 10 nM were dropped on Au nanoparticle-probe-modified IDE and incubated for 30 min. Then, the electrode was washed with PBS, and current changes were recorded. The difference in current from the blank was calculated and plotted in Excel to calculate the miRNA-363 limit of detection.

2.6 | Quantification of the miRNA-363 target in spiked human serum

miRNA-363 target spiked serum (1:100 dilution) was quantified on the Au nanoparticle-probe attached electrode surface. For this experiment, miRNA-363 concentrations from 100 aM to 10 nM were diluted in human serum, dropped on the Au nanoparticle-probe attached electrode, and incubated for 30 min. Then, the electrode was washed with PBS, and current changes were recorded.

2.7 | Comparison of control and specific experiments

Specific detection of miRNA-363 on Au nanoparticle-DNA attached electrode was confirmed by control experiments with unrelated miRNA sequences miRNA-21 and with a random sequence of miRNA-363 target DNA. Control sequences were dropped on the Au nanoparticle-probe attached electrode and rested for 30 min. Current changes were recorded for each concentration and compared with the specific detection of miRNA-363 DNA.

To confirm the reproducibility of the IDE, the same functionalization process was conducted with four different IDE electrodes from the same batch, and the current responses were recorded. The current response for the bare electrode, APTES, complementary probe, PEG-COOH, and target duplex formation were monitored and compared to confirm the reproducibility. The measurement system was operated by a picoammeter in the voltage range from 0 to 2 with an interval of 0.1 V. All experimental conditions were maintained as wet at room temperature, and surface washings were performed between each surface modification or interaction using 10 reaction volumes of 10 mM PBS (pH 7.4). The sensing devices were from the same batch of fabrication with similar dimensions.

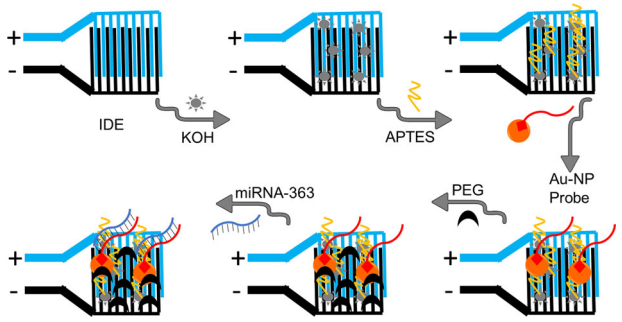

FIG 1 Graphical diagram for miRNA-363 target detection on the Au nanoparticle-probe-modified electrode. The Au nanoparticle probe was attached to IDE using an amine linker and then allowed to hybridize with the target with its complementary probe.

3 | RESULTS AND DISCUSSION

Figure 1 shows a schematic illustration of miRNA-363 target identification on the Au nanoparticle-probe-modified electrode. The Au nanoparticle probe was attached to the electrode using an amine linker and then allowed to hybridize to the target with a complementary probe. When hybridization occurs, nucleic acids have a negative net charge, changing the negative charge on the electrode surface. This process changes the response of the current before and after the hybridization of the target with the immobilized complementary probe with the detection mechanism of miRNA-363. Differences in current help to measure the hybridization process and quantify the target for miRNA-363. In this detection process, complementary immobilization on the electrode plays a vital role in improving the sensing of the target. The higher and proper immobilization improves the target identification and lowers the detection limit of the target. The Au nanoparticle attached probe helps to immobilize the higher number of target sequences on the electrode surface and hybridize with larger sequences, increasing the current responses and lowering the detection limit.[40] Further Au nanoparticles increase the current flow upon binding of biomolecules on the electrode, helping to quantify the miRNA-363 target at lower levels and diagnose glioma-associated problems. This sensor works based on the dipole moment between two electrodes due to changes in the ions on the sensing surface by molecular immobilization or interaction. When molecular immobilization or interaction occurs, the responses are revealed by the signal output changes.

3.1 | Functionalizing electrode by the complementary probe on IDE through Au nanoparticle

The complementary probe was functionalized on the electrode through Au nanoparticles as the linker. The current response for the functionalization process was recorded to confirm the attachment of the probe to the electrode (Figure 2A). The figure shows the increment of current responses after each process of biomolecular immobilization. The current response of the bare electrode was 1.37E-09 A, which changed to 4.21 E-08 A after modifying the electrode with amine by APTES. Furthermore, Au nanoparticle-probe immobilization increases the current responses drastically to 7.08 E-07 A. The difference in current after adding Au nanoparticle-probe was 6.659 E-07 A; this higher current change was recorded due to the larger number of probe attachments on the electrode through Au nanoparticles (Figure 2B). After probe attachment, the excess APTES surface was inactivated using PEG-COOH. Several studies have shown that amine surfaces easily attract biomolecules through electrostatic interactions and lead the electrode to give a false-positive result. Therefore, it is mandatory to cover the amine surface before target identification. PEG-based polymers are a great source for sensor surface functionalization and are commonly used as linkers and blocking agents. Herein, PEG-COOH blocks the uncovered amine surfaces and reduces the signal-to-noise ratio. PEG mediates the proper alignment of biomolecules for their interactions and neutralizes the surface charges.[41,42]

3.2 | miRNA-363 target quantification

miRNA-363 target DNA was quantified by its complementary probe on an interdigitated electrode. Targets from 1 fM to 100 pM were dropped individually on complementary probe-attached electrodes, and the current was recorded. The current response was changed from 7.94 E-07 to 1.81 E-06 A after dropping 1 fM of the target (Figure 3A). The difference in current was calculated to be 0.17 E-07 A. Furthermore, when target concentrations were increased to 10 fM, 100 fM, 1 pM, 10 pM, and 100 pM, currents were increased to 4.78 E-06, 7.01 E-06, 1.03 E-05, and 1.27 E-05 A, respectively. A gradual increase in current was noted when increasing the target concentrations (Figure 3B). The differences in current for 10 fM, 100 fM, 1 pM, 10 pM, and 100 pM target sequences were 2.092, 4.772, 7.0, 10.2 and 12.6 E-05 A. The differences were plotted as a linear graph in an

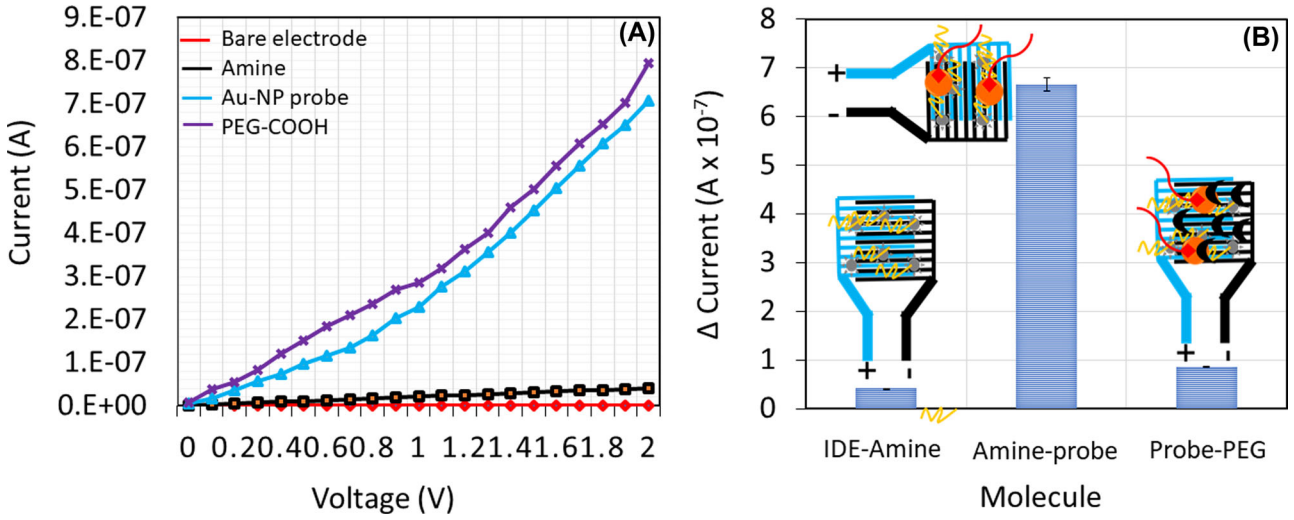

FIG 2 (A) Complementary probe functionalization on IDE. The increments in current responses after each process of biomolecular immobilization are shown. (B) Current changes for the functionalization process on IDE. Higher current changes were recorded due to the larger number of probe attachments on the electrode through Au nanoparticles. The inset is the diagrammatic representation. The data were averaged from three independent experiments.

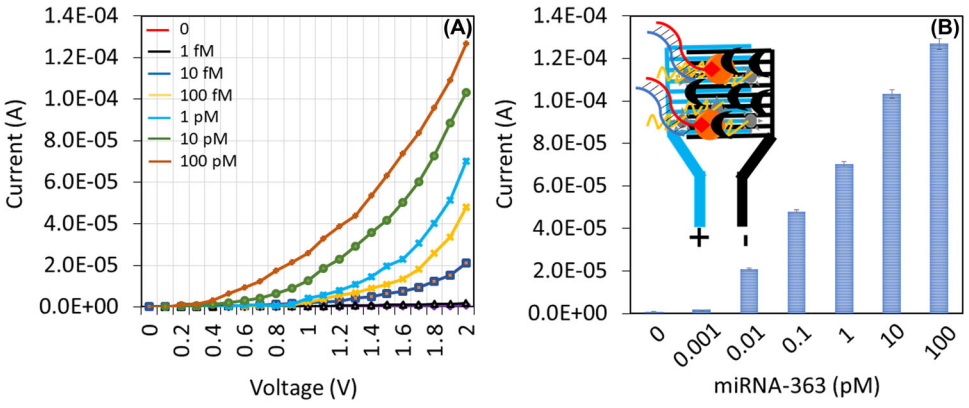

FIG 3 (A) miRNA-363 target quantification. Target concentrations from 1 fM to 100 pM were placed individually on complementary probe attached electrodes. Current changes were noted for all target concentrations. (B) Graph for responses in current with each target concentration. Gradual increments of current were noted when increasing the target concentration. The inset is the diagrammatic representation. The data were averaged from three independent experiments.

Excel sheet, and the limit of detection was found to be in the range between 1 and 10 fM with an R^2 value of 0.996 (Figure 4A).

3.3 | Current comparison for control and specific experiments

Specific miRNA-363 detection on the Au nanoparticle-probe attached electrode was compared with control experiments performed with unrelated sequences. Instead of the miRNA-363 target, miRNA-21 and random sequences were added to the complementary probe-modified electrode. Current changes were recorded for each experiment and compared with the specific detection of the miRNA-363 target. As shown in Figure 4B, the control sequences did not increase the current responses; simultaneously, a similar concentration of the miRNA-363 target showed a clear increase in the current responses. This experiment confirms the specific interaction of the miRNA-363 target with the complementary probe on IDE.

To confirm the reproducibility of the IDE surfaces, similar functionalization processes and target identification were performed with four different IDE electrodes, and the current responses were compared. The current responses for the bare electrode, APTES, complemen-

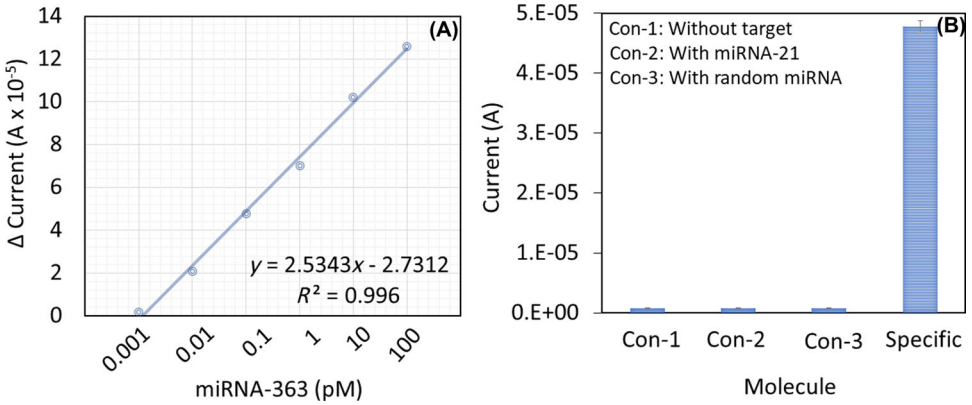

FIG 4 (A) Limit of detection of target sequences. The differences were plotted in a linear graph with an Excel sheet, and the limit of detection was 10 fM with an R^2 value of 0.996. (B) Specific miRNA-363 detection on the Au nanoparticle-probe attached electrode. Control sequences against miRNA-21 did not increase the current responses; simultaneously, a similar concentration of the miRNA-363 target displayed a clear increase in current responses. The data were averaged from three independent experiments.

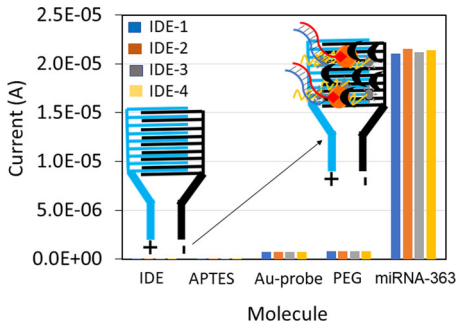

FIG 5 Reproducibility of IDE. To confirm the reproducibility of the IDE, the same functionalization process and target identification were performed with four different IDE electrodes. The current responses for all of the biomolecular immobilizations were close and did not show significant differences in current responses. The inset is the diagrammatic representation.

tary probe, PEG-COOH, and target sequence displayed close responses and did not show much difference in current responses (Figure 5). This result confirms the reproducibility of target DNA identification on IDE.

4 | Conclusion

Glioma is a life-threatening tumor that originates in the brain and affects its function. Identifying and quantifying glioma biomarkers helps to diagnose glioma and its condition. This study focused on identifying the miRNA-363 target, which was found to be a suitable biomarker for glioma. The interdigitated electrode sensor was modified with the Au nanoparticle-conjugated complementary probe through the amine linker, and then the hybridization of the target and complementary probe was monitored by the current responses. The current responses were increased after enhancing the target sequence, and the limit of target detection was in the range between 1 and 10 fM from a linear regression graph R^2 value of 0.996. Furthermore, control experiments with unknown sequences did not increase the current, indicating specific miRNA-363 target detection. This miRNA biosensor quantifies miRNA-363 at a lower level and helps in diagnosing glioma. The strategy with this analysis can be implemented for other nucleic acid or miRNA interactions by complementation. Furthermore, other biomolecular interactions with similar functionalization can be performed.

ORCID

Xiuhua Yang https://orcid.org/0000-0002-0199-7629

REFERENCES

1. Thakur A, Sidu RK, Zou H, Alam MK, Yang M, Lee Y. Inhibition of glioma cells' proliferation by doxorubicin-loaded exosomes via microfluidics. Int J Nanomed. 2020;15:8331–43.
2. Montano N, D'Alessandris QG, Izzo A, Fernandez E, Pallini R. Biomarkers for glioblastoma multiforme: status quo. J Clin Transl Res. 2016;2:3–10.
3. Yang Z, Zhang N, Shen Z, Bai S, Shi M, Yin L, et al. Markers for early diagnosis and post-operative recurrence monitoring of bladder cancer. Cancer Plus. 2020;2:43–52.
4. Liu Q, Ding JJ, Liu FY, Jiang ZZ, Li L, Xiao XB, et al. The novel biomarkers in diagnosis of prostate cancer. Cancer Plus. 2019;1:8–16.
5. McGill MR, Jaeschke H. Biomarkers of mitotoxicity after acute liver injury: further insights into the interpretation of glutamate dehydrogenase. J Clin Transl Res. 2021;7:61–65.
6. García-Romero N, Carrión-Navarro J, Esteban-Rubio S, Lázaro-Ibáñez E, Peris-Celda M, Alonso MM, et al. DNA sequences within glioma-derived extracellular vesicles can cross the intact blood–brain barrier and be detected in peripheral blood of patients. Oncotarget. 2017;8:1416–28.

7. Lang H-L, Hu G-W, Zhang B, Kuang W, Chen Y, Wu L, et al. Glioma cells enhance angiogenesis and inhibit endothelial cell apoptosis through the release of exosomes that contain long non-coding RNA CCAT2. Oncol Rep. 2017;38:785–98.
8. Simons M, Raposo G. Exosomes-vesicular carriers for intercellular communication. Curr Opin Cell Bio. 2009;21:575–81.
9. Malsagova KA, Pleshakova TO, Galiullin RA, Kozlov AF, Romanova TS, Shumov ID, et al. Soi-nanowire biosensor for the detection of glioma-associated mirnas in plasma. Chemosensors. 2020;8:1–11.
10. Lin J, Ma L, Zhang D, Gao J, Jin Y, Han Z, et al. Tumour biomarkers—tracing the molecular function and clinical implication. Cell Prolif. 2019;52:e12589.
11. Carrington JC, Ambros V. Role of microRNAs in plant and animal development. Science. 2003;301:336–8.
12. Knoka E, Trusinskis K, Mazule M, Briede I et al., Circulating plasma microRNA-126, -145 and -155 and their association with atherosclerotic plaque characteristics. J Clin Transl Res. 2019;5:60–67.
13. Lu J, Getz G, Miska EA, Alvarez-Saavedra E, Lamb J, Peck D, et al. MicroRNA expression profiles classify human cancers. Nature. 2005;435:834–8.
14. Lv D-K, Bai X, Li Y, Ding X-D, Ge Y, Cai H, et al. Profiling of cold-stress-responsive miRNAs in rice by microarrays. Gene. 2010;459:39–47.
15. Calin GA, Ferracin M, Cimmino A, Di Leva G, Shimizu M, Wojcik SE, et al. A MicroRNA signature associated with prognosis and progression in chronic lymphocytic leukemia. N Engl J Med. 2005;353:1793–801.
16. Volinia S, Calin GA, Liu C-G, Ambs S, Cimmino A, Petrocca F, et al. A microRNA expression signature of human solid tumors defines cancer gene targets. Proc Natl Acad Sci U S A. 2006;103:2257–61.
17. Chan JA, Krichevsky AM, Kosik KS. MicroRNA-21 is an antiapoptotic factor in human glioblastoma cells. Cancer Res. 2005;65:6029–33.
18. Conti A, Aguennouz MH, La Torre D, Tomasello C, Cardali S, Angileri FF, et al. miR-21 and 221 upregulation and miR-181b downregulation in human grade II-IV astrocytic tumors. J Neurooncol. 2009;93:325–32.
19. Ciafrè SA, Galardi S, Mangiola A, Ferracin M, Liu C-G, Sabatino G, et al. Extensive modulation of a set of microRNAs in primary glioblastoma. Biochem Biophys Res Commun. 2005;334:1351–8.
20. Conti A, Romeo SG, Cama A, La Torre D, Barresi V, Pezzino G, et al. MiRNA expression profiling in human gliomas: upregulated miR-363 increases cell survival and proliferation. Tumor Biol. 2016;37:14035–48.
21. Zhang R, Wang S, Huang X, Yang Y, Fan H, Yang F, et al. Gold-nanourchin seeded single-walled carbon nanotube on voltammetry sensor for diagnosing neurogenerative Parkinson's disease. Anal Chim Acta. 2020;1094:142–50.
22. Zhang W, Li K, Guo J, Ma T, Wang D, Shi S, et al. Sensitive identification of prostate-specific antigen by iron oxide nanoparticle antibody conjugates on the gap-finger electrode surface. Biotechnol Appl Biochem. 2021;68:896–901.
23. Hou Y, Wang W, Bártolo P. Investigating the effect of carbon nanomaterials reinforcing poly(ε-Caprolactone) printed scaffolds for bone repair applications. Int J Bioprinting. 2020;6:1–9.
24. Shuai C, Li Y, Yang W, Yu L, et al. Graphene oxide induces ester bonds hydrolysis of poly-L-lactic acid scaffold to accelerate degradation. Int J Bioprinting. 2020:6:91–104.
25. Koch L, Brandt O, Deiwick A, Chichkov B. Laser assisted bioprinting at different wavelengths and pulse durations with a metal dynamic release layer: a parametric study. Int J Bioprinting. 2017;3:42–53.
26. Carrasco-esteban E, Domínguez-rullán JA, Barrionuevo-castillo P, Pelari-mici L, López-campos F. Current role of nanoparticles in the treatment of lung cancer. J Clin Transl Res. 2021;7:140–55.
27. Rueda-Gensini L, Serna JA, Cifuentes J, Cruz JC, Muñoz-Camargo C. Graphene oxide-embedded extracellular matrix-derived hydrogel as a multiresponsive platform for 3D bioprinting applications. Int J Bioprinting. 2021;7:1–16.
28. Chen S, Jang TS, Pan HM, Jung HD, et al. 3D freeform printing of nanocomposite hydrogels through in situ precipitation in reactive viscous fluid. Int J Bioprinting. 2020;6:1–21.
29. Zhang Y, Attarilar S, Wang L, Lu W, Yang J, Fu Y. A review on design and mechanical properties of additively manufactured NiTi implants for orthopedic applications. Int J Bioprinting. 2021;7:15–42.
30. Ding Y, Tian Q, Dong Y, Xing L, Gopinath SCB, Mao Y. Gold-silane complexed antibody immobilization on polystyrene ELISA surface for enhanced determination of matrix Metalloproteinase-9. Process Biochem. 2021;100:231–6.
31. Gopinath SCB, Lakshmipriya T, Awazu K. Colorimetric detection of controlled assembly and disassembly of aptamers on unmodified gold nanoparticles. Biosens Bioelectron. 2014;51:115–23.
32. Letchumanan I, Md Arshad MK, Gopinath SCB, Rajapaksha RDAA, Balakrishnan SR. Comparative analysis on dielectric gold and aluminium triangular junctions: impact of ionic strength and background electrolyte by pH variations. Sci Rep. 2020;10:6783.
33. Gu D, Zhang Q, Guo J, Ma T, Li H, Ji J, et al. Gold nanomaterial hybrid on PEGylated metal oxide interdigitated mini-electrode surface to diagnose prostate cancer. Nano. 2020;15:2050154.
34. Lakshmipriya T, Horiguchi Y, Nagasaki Y. Co-immobilized poly(ethylene glycol)-*block*-polyamines promote sensitivity and restrict biofouling on gold sensor surface for detecting factor IX in human plasma. Analyst. 2014;139:3977–85.
35. Lakshmipriya T, Fujimaki M, Gopinath SCB, Awazu K, Horiguchi Y, Nagasaki Y. A high-performance waveguide-mode biosensor for detection of factor IX using PEG-based blocking agents to suppress non-specific binding and improve sensitivity. Analyst. 2013;138:2863.
36. Liu Z, Gopinath SCB, Wang Z, Li Y, Anbu P, Zhang W. Zeolite-iron oxide nanocomposite from fly ash formed a 'clubbell' structure: integration of cardiac biocapture macromolecules in serum on microelectrodes. Microchim Acta. 2021;188:187.
37. Yu Z, Gopinath SCB, Lakshmipriya T, Anbu P. Single-walled carbon nanotube-gold urchin nanohybrid for identifying gastric cancer on dimicroelectrodes junction. J Taiwan Inst Chem Eng. 2021;121:108–14.
38. Wang Y, Guo Y, Lu J, Sun Y, Yu X, Gopinath SCB, et al. Nanodetection of head and neck cancer on titanium oxide sensing surface. Nanoscale Res Lett. 2020;15:33.
39. Adam H, Gopinath SCB, Arshad MKM, Parmin NA, Hashim U. Distinguishing normal and aggregated alpha-synuclein interac-

tion on gold nanorod incorporated zinc oxide nanocomposite by electrochemical technique. Int J Biol Macromol. 2021;171:217–24.
40. Gopinath SCB, Perumal V, Kumaresan R, Lakshmipriya T, Rajintraprasad H, Rao BS, et al. Nanogapped impedimetric immunosensor for the detection of 16 kDa heat shock protein against *Mycobacterium tuberculosis*. Microchim Acta. 2016;183:2697–703.
41. Lakshmipriya T, Fujimaki M, Gopinath SCB, Awazu K, Horiguchi Y, Nagasaki Y. A high-performance waveguide-mode biosensor for detection of factor IX using PEG-based blocking agents to suppress non-specific binding and improve sensitivity. Analyst. 2013;138:2863–70.
42. Lakshmipriya T, Horiguchi Y, Nagasaki Y. Co-immobilized poly(ethylene glycol)-*block*-polyamines promote sensitivity and restrict biofouling on gold sensor surface for detecting factor IX in human plasma. Analyst. 2014;139:3977–85.

How to cite this article: Li Z, Wan X, Li M, He Q, Yang H, Zhang W, et al. Evaluating glioma-associated microRNA by complementation on a biological nanosensor. Biotechnology and Applied Biochemistry. 2022;1–8. https://doi.org/10.1002/bab.2374